

Two-neutron halo nuclei in one dimension: dineutron correlation and breakup reaction

K. Hagino¹, A. Vitturi^{2,3}, F. Pérez-Bernal⁴, and H. Sagawa⁵

¹ Department of Physics, Tohoku University, Sendai, 980-8578, Japan

E-mail: hagino@nucl.phys.tohoku.ac.jp

² Dipartimento di Fisica Galileo Galilei, Università di Padova, I-35131 Padova, Italy

³ INFN, Sezione di Padova, I-35131 Padova, Italy

⁴ Departamento de Física Aplicada, Facultad de Ciencias Experimentales,
Universidad de Huelva, 21071 Huelva, Spain

⁵ Center for Mathematics and Physics, University of Aizu, Aizu-Wakamatsu,
965-8580, Fukushima, Japan

Abstract. We propose a simple schematic model for two-neutron halo nuclei. In this model, the two valence neutrons move in a one-dimensional mean field, interacting with each other via a density-dependent contact interaction. We first investigate the ground state properties, and demonstrate that the dineutron correlation can be realized with this simple model due to the admixture of even- and odd-parity single-particle states. We then solve the time-dependent two-particle Schrödinger equation under the influence of a time-dependent one-body external field, in order to discuss the effect of dineutron correlation on nuclear breakup processes. The time evolution of two-particle density shows that the dineutron correlation enhances the total breakup probability, especially for the two-neutron breakup process, in which both the valence neutrons are promoted to continuum scattering states. We find that the interaction between the two particles definitely favours a spatial correlation of the two outgoing particles, which are mainly emitted in the same direction.

PACS numbers: 21.10.Gv, 25.60.Gc, 21.60.Cs, 24.10.-i

Submitted to: *J. Phys. G: Nucl. Phys.*

1. Introduction

Neutron-rich nuclei have attracted much interest during the past decades[1, 2, 3, 4, 5, 6], and this will continue to be so due to new generation radioactive beam facilities in the world. These nuclei are characterized by a small binding energy, and many new features originating from the weakly bound property have been found. A halo and skin structures with a large spatial extension of the density distribution[7], a narrow momentum distribution [8], a modification of shell structure and magic numbers[9], and strong concentration of electric dipole ($E1$) transition at low excitation energies [10, 11, 12], are well-known examples.

Among neutron-rich nuclei, two-neutron halo nuclei are particularly intriguing systems to study. Their structure has often been described as a three-body system consisting of two valence neutrons interacting with each other and with the core nucleus [4, 5, 13, 14]. Some light neutron-rich nuclei, such as ^{11}Li and ^6He , do not have a bound state in the two-body subsystem with a valence neutron and a core nucleus. These nuclei are referred to as Borromean nuclei, and their properties have been studied extensively both experimentally [1, 2, 7, 8, 11, 12] and theoretically [3, 4, 5, 6, 15, 16, 17, 18]. Nuclear breakup reactions of Borromean nuclei have also been investigated by the continuum-discretized-coupled-channels (CDCC) method [19, 20, 21, 22, 23] and by the eikonal method [24, 25, 26].

One of the most important current open questions concerning the Borromean nuclei is to clarify the characteristic nature of correlations between the two valence neutrons, which do not form a bound state in the vacuum. A strong dineutron correlation, where the two neutrons take a spatially compact configuration, has been theoretically predicted [3, 4, 5, 16, 27, 28, 29, 30]. Although the recent experimental observation of the strong low-lying dipole strength distribution in the ^{11}Li nucleus [12] has provided an experimental signature of the existence of dineutron correlation in this nucleus, its direct evidence has not yet been obtained.

The pair transfer reaction is another promising way to probe the dineutron correlation, as the cross section is known to be sensitive to the pairing correlation [31, 32]. However, the reaction dynamics is rather complicated and the role of dineutron in the pair transfer reaction has not yet been fully clarified, although experimental studies on pair transfer reaction with exotic nuclei have been initiated recently [33, 34, 35]. Apparently, it is urged to construct a theoretical framework for pair transfer which fully takes into account the pairing correlation and the dineutron correlation in its consequence.

The aim of this paper is to develop a simple toy model for two-neutron halo nuclei. Albeit its schematic nature, such model is rather useful as it allows detailed studies on the static and dynamical properties of two-neutron halo nuclei. A schematic model is also useful to deepen our understanding of two-neutron halo nuclei by providing intuitive pictures of several dynamical processes. To this end, we consider a three-body model in which the motion of two valence neutrons is confined within one-dimensional spatial space. The neutrons are assumed to move in a one-dimensional Woods-Saxon potential, while interacting with each other via a two-body interaction, which we take a density-dependent contact interaction [4, 15, 16]. This is a natural extension of the model developed in Ref. [36] for a one-neutron halo nucleus. We apply the model to the ground state as well as to a nuclear breakup process of a loosely-bound two-neutron halo nucleus, leaving an application to the pair transfer process in a separate publication. In passing, a similar one-dimensional three-body model has been used in atomic physics, in order to discuss *e.g.*, the mechanism of the double ionization process of He atom by intense laser fields [37, 38, 39].

The paper is organized as follows. In Sec. II, we detail the one-dimensional three-

body model. In Sec. III, we apply the model to the ground state of a loosely-bound two-neutron halo nucleus and discuss the dineutron correlation. In Sec. IV, we consider the two-neutron halo nucleus under the influence of a time-dependent external field. We solve the time-dependent Schrödinger equation in one-dimensional coordinate space and discuss the time evolution of the two-particle wave function. We then summarize the paper in Sec. V.

2. One-dimensional three-body model

We consider a two-neutron halo nucleus in a one dimensional space. Denoting the coordinate of the two neutrons by x_1 and x_2 , the three-body Hamiltonian reads,

$$H = -\frac{\hbar^2}{2m} \frac{d^2}{dx_1^2} + V(x_1) - \frac{\hbar^2}{2m} \frac{d^2}{dx_2^2} + V(x_2) + v_{nn}(x_1, x_2), \quad (1)$$

where m is the nucleon mass. Here, we neglect for simplicity the recoil kinetic energy of the core nucleus. $V(x)$ is the neutron-core potential, which we take the Woods-Saxon form[36],

$$V(x) = -\frac{V_0}{1 + e^{(|x|-R)/a}}. \quad (2)$$

v_{nn} is the neutron-neutron interaction. We take the density-dependent contact interaction for it, that is,

$$v_{nn}(x, x') = -g \left(1 - \frac{1}{1 + e^{(|x|-R)/a}} \right) \delta(x - x'), \quad (3)$$

where we assume that the density is given by the same functional form as the mean-field potential, Eq. (2). This is the so called surface type pairing interaction, which almost vanishes near the center of the core nucleus at $x \sim 0$. The density-dependent contact interaction has been successfully employed in the Hartree-Fock-Bogoliubov calculations for neutron-rich medium-heavy and heavy nuclei[28, 40], as well as in describing the structure of ^{11}Li and ^6He nuclei with the three-body model [4, 15, 16].

In order to obtain the ground state wave function of the two-neutron halo nucleus, we first solve the Schrödinger equation for the two-body subsystem,

$$\left[-\frac{\hbar^2}{2m} \frac{d^2}{dx^2} + V(x) - \epsilon_n \right] \phi_n(x) = 0. \quad (4)$$

Each eigenstate n is assumed to have a two-fold degeneracy, depending on the direction of the spin of neutron. The continuum states are discretized by putting the nucleus within a large box. Denoting the size of the box to be X_{box} , we impose the vanishing boundary condition $\phi_n(x) = 0$ at $x = \pm X_{\text{box}}$.

We expand the two-particle wave function $\Psi(x_1, x_2)$ with the single-particle wave functions $\phi_n(x)$ as

$$\Psi_{\text{gs}}(x_1, x_2) = \sum_{n \leq n'} \alpha_{nn'} \Psi_{nn'}(x_1, x_2), \quad (5)$$

where

$$\Psi_{nn'}(x_1, x_2) = \frac{1}{\sqrt{2(1 + \delta_{n,n'})}} [\phi_n(x_1)\phi_{n'}(x_2) + \phi_n(x_2)\phi_{n'}(x_1)] |S=0\rangle. \quad (6)$$

Here we have assumed that the spin of the two neutrons form the total spin of $S=0$ configuration, so that the wave function is symmetric with respect to the interchange of x_1 and x_2 . Notice that the Hamiltonian (1) conserves the parity. Since the ground state has positive parity, the expansion in Eq. (5) can therefore be restricted to the configurations where the states n and n' have the same parity. The expansion coefficients $\alpha_{nn'}$ are determined by diagonalizing the Hamiltonian matrix, whose matrix elements read,

$$\begin{aligned} \langle \Psi_{n_1 n_2} | H | \Psi_{n'_1 n'_2} \rangle &= (\epsilon_{n_1} + \epsilon_{n_2}) \delta_{n_1, n'_1} \delta_{n_2, n'_2} \\ &\quad - \frac{4g}{\sqrt{2(1 + \delta_{n_1, n_2})} \sqrt{2(1 + \delta_{n'_1, n'_2})}} \\ &\quad \times \int_{-\infty}^{\infty} dx \left(1 - \frac{1}{1 + e^{(|x|-R)/a}} \right) \phi_{n_1}^*(x) \phi_{n_2}^*(x) \phi_{n'_1}(x) \phi_{n'_2}(x). \end{aligned} \quad (7)$$

Once the ground state wave function $\Psi_{\text{gs}}(x_1, x_2)$ is obtained, the two-particle and one-particle densities can be constructed as

$$\rho_2(x_1, x_2) = |\Psi_{\text{gs}}(x_1, x_2)|^2, \quad (8)$$

and

$$\rho_1(x) = \int dx' \rho_2(x, x'), \quad (9)$$

respectively. The mean value of the neutron-neutron distance and the distance between the core and the center of mass of the two neutrons are also computed as

$$x_{\text{nn}} = \sqrt{\int_{-\infty}^{\infty} dx_1 dx_2 (x_1 - x_2)^2 \rho_2(x_1, x_2)}, \quad (10)$$

$$x_{\text{c2n}} = \sqrt{\int_{-\infty}^{\infty} dx_1 dx_2 \left(\frac{x_1 + x_2}{2} \right)^2 \rho_2(x_1, x_2)}, \quad (11)$$

respectively.

3. Ground state properties

We now apply the one-dimensional model to a weakly-bound two-neutron halo nucleus. To this end, we take $R = 1.27 \times 9^{1/3}$ fm, $V_0 = -50.085$ MeV, and $a=0.67$ fm for the Woods-Saxon potential, Eq. (2), in order to mimic the ^{11}Li nucleus. This potential possesses four bound single-particle states. We assume that the lowest three bound states are already occupied by the neutrons in the core nucleus, and exclude those states explicitly from the expansion in Eq. (5). In this way, the Woods-Saxon potential has effectively only one bound state with odd parity at $\epsilon_{\text{WS}} = -0.15$ MeV. That is, the three-body system is bound by 0.3 MeV without the pairing interaction. Although we

could set up a situation in which there is no bound state in a Woods-Saxon potential, we introduce a loosely bound single-particle state in order to mock up a resonance state, which plays an important role in the ^{11}Li and ^6He nuclei [17].

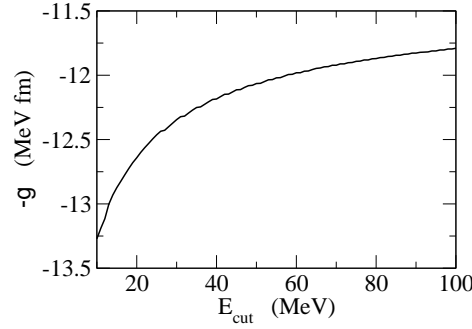


Figure 1. The dependence of the strength of the pairing interaction g on the cutoff energy, E_{cut} . For each E_{cut} , the strength g is adjusted in order to yield the ground state at $E_{\text{g.s.}} = -1$ MeV.

It is well known that a contact interaction has to be supplemented with an energy cutoff, E_{cut} [4, 15]. For a three-dimensional case, the strength of the pairing interaction, g , is related to the cutoff energy, E_{cut} , via a scattering length a_{nn} for the $n+n$ scattering [4, 15]. On the other hand, for a one-dimensional case, we simply vary the value of g for each cutoff energy (with keeping the Woods-Saxon potential well) in order to reproduce a given ground state energy, since it is not straightforward to define the phase shift for a one-dimensional scattering problem. Figure 1 shows the dependence of g on E_{cut} for the ground state energy of $E_{\text{g.s.}} = -1$ MeV, obtained by taking the configurations in Eq. (5) which satisfy $\epsilon_n + \epsilon_{n'} \leq E_{\text{cut}}$. One notices that the dependence is rather weak. In this paper, we arbitrarily take the cutoff energy to be 30 MeV, that corresponds to $g = -12.35$ MeV·fm for $E_{\text{g.s.}} = -1$ MeV.

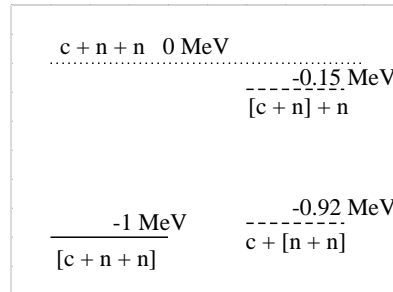


Figure 2. The energy spectrum for the model Hamiltonian used in this paper. The energies are measured from the threshold of a three-body scattering state. The three-body bound state, $[c+n+n]$, is located at $E = -1$ MeV. The $[n+n]$ and $[c+n]$ are two-body bound states for the two-neutron ($n+n$) and the core+neutron ($c+n$) systems, respectively.

It is important to notice that a one-dimensional delta function potential $v(x) =$

$-g\delta(x)$ always holds a bound state at $E = -mg^2/4\hbar^2$ for a two-neutron system even with an infinitesimally small attraction g [41]. For our choice of $g = -12.35$ MeV·fm, a dineutron is thus bound by 0.92 MeV. See Fig.2 for a spectrum for the three-body system considered in this paper. There is no bound excited state below the threshold of the core nucleus + a bound dineutron at $E = -0.92$ MeV. Thus, the ground state in the present model has an extremely small separation energy from the threshold for the dineutron breakup, *i.e.*, less than 100 keV. Since the dineutron is bound, our calculations correspond to a limit of strong neutron-neutron interaction in a three-dimensional case. Alternatively, our calculations also have a similarity to ${}^6\text{Li}$ in which a bound deuteron may exist in the channel of ${}^6\text{Li} = \alpha + p + n$.

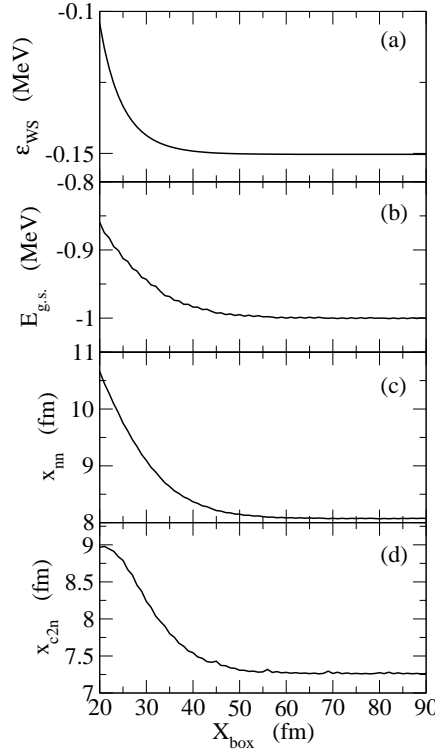


Figure 3. The energy of the last bound single-particle level (Fig. 3(a)), the ground state energy of the three-body system (Fig. 3(b)), the neutron-neutron mean distance (Fig. 3(c)), and the core-dineutron mean distance (Fig. 3(d)) as a function of the size of the box, X_{box} .

Figure 3 shows several quantities for the ground state of the three-body Hamiltonian, Eq. (1), as a function of the size of the box, X_{box} . Figs. 3(a), 3(b), 3(c), and 3(d) are for the single-particle energy of the last bound level, the ground state energy of the three-body system, the neutron-neutron root mean square distance, and the mean distance between the core and the center of mass of the two neutrons, respectively. These quantities are almost converged at $X_{\text{box}} \sim 50$ fm. For a Borromean system, it was shown that the convergence of the ground state wave function is much slower than the ground state energy, especially in the tail region[42, 43]. For the example

shown in Fig. 3, in which there is a bound single-particle state, we have confirmed that the wave function has also converged at $X_{\text{box}} \sim 50$ fm. In the calculations shown in this paper, we take the box size to be $X_{\text{box}}=90$ fm.

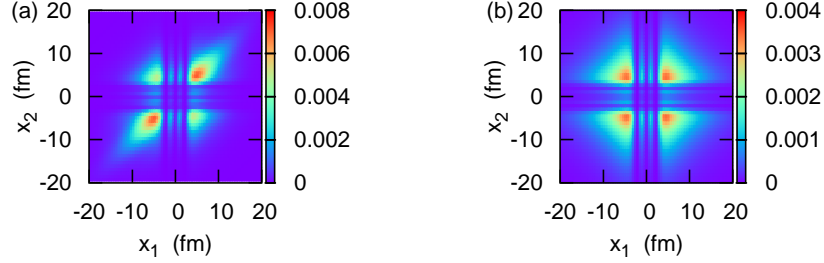


Figure 4. (Color online) The two-particle density for the correlated (Fig. 4(a)) and the non-correlated (Fig. 4(b)) ground states of a one-dimensional three-body model.

Figure 4(a) shows the two-particle density of the ground state. The density distribution is largely concentrated along the line of $x_1 \sim x_2$, that is nothing but the manifestation of strong dineutron correlation discussed in Refs.[4, 5, 16, 27, 28, 29, 30]. The correlation largely hinders the density along the $x_1 = -x_2$ line, and only the peaks along $x_1 \sim x_2$ survive. When the pairing interaction is switched off, the two-particle density becomes that shown in Fig. 4(b). The density for the non-correlated ground state is symmetric with respect to the transformation of $x_1 \rightarrow -x_1$ ($x_2 \rightarrow -x_2$) for a fixed value of x_2 (x_1), and it has therefore four symmetric peaks. See Ref. [44] for a similar figure for the ^{11}Li nucleus.

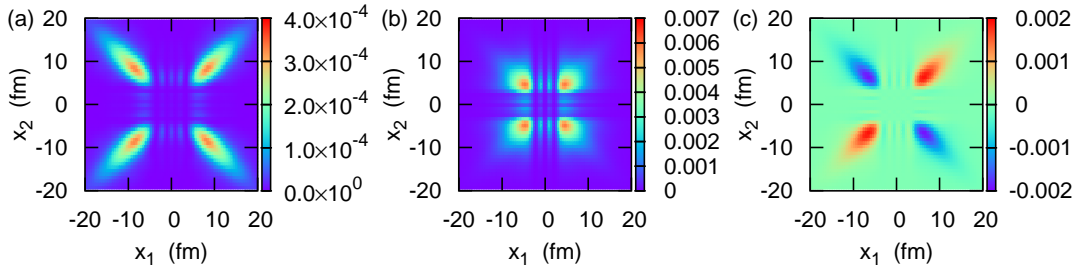


Figure 5. (Color online) The decomposition of the correlated two-particle density into the even-parity contribution (Fig. 5(a)), the odd-parity contribution (Fig. 5(b)), and the interference between the even and odd parity contributions (Fig. 5(c)).

It is well known that the dineutron correlation is caused by the admixture of many single-particle states with different parity [29, 45]. In order to demonstrate it explicitly, we decompose the ground state wave function, Eq. (5), into two components,

$$\Psi_{\text{gs}}(x_1, x_2) = \Psi_{\text{ee}}(x_1, x_2) + \Psi_{\text{oo}}(x_1, x_2), \quad (12)$$

where $\Psi_{ee}(x_1, x_2)$ and $\Psi_{oo}(x_1, x_2)$ consist only of the even-parity and the odd-parity single-particle states, respectively. Assuming that Ψ_{ee} and Ψ_{oo} are both real, the two-particle density then reads,

$$\rho_2(x_1, x_2) = |\Psi_{ee}(x_1, x_2)|^2 + |\Psi_{oo}(x_1, x_2)|^2 + 2\Psi_{ee}(x_1, x_2)\Psi_{oo}(x_1, x_2). \quad (13)$$

Fig. 5 shows each of the components separately (see also Fig. 12 in Ref. [29]). With only even or odd parity single-particle states, the density distribution has four symmetric peaks as in the non-correlated case shown in Fig. 4(b). $|\Psi_{oo}|^2$ is much more compact than $|\Psi_{ee}|^2$ because the former contains the bound single-particle state. It is clearly seen in Fig. 5(c) that the localization of the two-neutron pair along the line $x_1 = x_2$ emerges only with the interference between the even and odd parity states[29, 45].

This can be understood easily as follows. Because the nuclear interaction is short ranged, the main contribution comes from $n = n'$ in Eq. (5). Suppose that there are only one even-parity single-particle state $\phi_e(x)$ and one odd-parity state, $\phi_o(x)$. If we write the ground state wave function as

$$\Psi_{\text{g.s.}}(x, x') = \alpha \phi_e(x)\phi_e(x') + \beta \phi_o(x)\phi_o(x'), \quad (14)$$

the two-particle density reads

$$\begin{aligned} \rho_2(x, x') &= \alpha^2 |\phi_e(x)\phi_e(x')|^2 + \beta^2 |\phi_o(x)\phi_o(x')|^2 \\ &\quad + 2\alpha\beta \phi_e(x)\phi_e(x')\phi_o(x)\phi_o(x'). \end{aligned} \quad (15)$$

As we prove in the Appendix by using the two-level model, α and β have the same sign for the density-dependent pairing interaction. The first and the second terms in this equation are positive definite. On the other hand, the third term is positive for $x = x'$, while it is negative for $x = -x'$ as $\phi_e(-x) = \phi_e(x)$ and $\phi_o(-x) = -\phi_o(x)$. Therefore, the interference term is destructive and decreases the two-body density along the $x = -x'$ line, while it is constructive and enhances the density along the $x = x'$ line.

In the past, the dineutron correlation was discussed using several representations. In Refs. [4, 28, 44], the density distribution of the second neutron was investigated when the first neutron was fixed at a certain position. In Refs. [5, 29, 27, 45, 46, 47, 48, 49], the two-particle density was plotted as a function of the relative distance between the neutrons, $\mathbf{r} = \mathbf{r}_1 - \mathbf{r}_2$, and the center of mass coordinate, $\mathbf{R} = (\mathbf{r}_1 + \mathbf{r}_2)/2$. In Ref. [16], by setting $r_1 = r_2 = r$ the two-particle density was plotted as a function of the core-neutron distance, r , and the opening angle between the two neutrons, θ_{12} . Although all the representations are useful to reveal the strong dineutron correlation, they have advantages and disadvantages. For instance, it is not easy to explore all the position of the first neutron in the first representation, and the configurations with $r_1 \neq r_2$ are neglected in the third representation. These can be avoided with the second representation, but it is more intuitive to use directly the coordinates \mathbf{r}_1 and \mathbf{r}_2 , rather than \mathbf{r} and \mathbf{R} , especially when one has to consider also the angular part of \mathbf{r} and \mathbf{R} . The one-dimensional model removes these inconveniences, yielding a transparent picture for the two-particle density distribution.

4. Nuclear Breakup process

Let us next discuss the time evolution of the two-particle wave function in the presence of an external field acting on each particle. As the external field, we take [36]

$$V_{\text{ext}}(x_1, x_2, t) = \sum_{i=1,2} V_c e^{-t^2/2\sigma_t^2} e^{-(x_i-x_0)^2/2\sigma_x^2}, \quad (16)$$

with the parameters of $V_c=3$ MeV, $\sigma_t = 2.1\hbar/\text{MeV}$, and $\sigma_x=2.2$ fm. In order to investigate the time evolution, we solve the time-dependent two-particle Schrödinger equation,

$$i\hbar \frac{\partial}{\partial t} \Psi(x_1, x_2, t) = [H + V_{\text{ext}}(x_1, x_2, t)] \Psi(x_1, x_2, t), \quad (17)$$

with the initial condition of

$$\Psi(x_1, x_2, t_0) = \Psi_{\text{gs}}(x_1, x_2), \quad (18)$$

at the initial time t_0 . We orthonormalize the wave function to the occupied states using the projection procedure at each time step during the time evolution. In the calculations shown below, we take $ct_0 = -400$ fm, and use the implicit method [50] for the time propagation. We consider the symmetric perturbation, that is, $x_0 = 0$ in Eq. (16). We have confirmed that our conclusions remain qualitatively the same (except for the asymmetry in the two-particle density distribution along the $x_1 = x_2$ line) even if we choose an asymmetric perturbation [36], *e.g.*, with $x_0 = 2$ fm.

Figures 6(a), 6(b), 6(c), and 6(d) show the two-particle density at $ct = -400, 0, 300$, and 600 fm, respectively. As the time evolves, the extension of the peaks along the $x_1 = x_2$ line increases significantly. This is in marked contrast to the uncorrelated case shown in Figs. 7(a), 7(b), 7(c), and 7(d). In the uncorrelated case, the two-particle density expands democratically, indicating that there is the equal probability of emission of the two neutrons in the opposite directions to that in the same direction.

The corresponding current distributions,

$$j_i(x_1, x_2, t) = \frac{\hbar}{2im} \left(\Psi^*(x_1, x_2, t) \frac{\partial}{\partial x_i} \Psi(x_1, x_2, t) - \Psi(x_1, x_2, t) \frac{\partial}{\partial x_i} \Psi^*(x_1, x_2, t) \right), \quad (19)$$

are shown in Figs. 6(e-g) and 7(e-g) for the correlated and the uncorrelated cases, respectively. For the correlated case, the main flows are the outgoing flows along the $x_1 = x_2$ line, as one can infer from Figs. 6(b), 6(c), and 6(d). For the uncorrelated case, on the other hand, there are four symmetric outgoing flows that correspond to the expanding density distribution shown in Figs. 7(b), 7(c), and 7(d).

In order to see more clearly the time evolution of the breakup fragments, we project the two-particle wave function at each time t onto the component which is orthogonal to the ground state. That is,

$$\Psi_{\text{bu}}(x_1, x_2, t) = \Psi(x_1, x_2, t) - \langle \Psi_{\text{gs}} | \Psi(t) \rangle \Psi_{\text{gs}}(x_1, x_2). \quad (20)$$

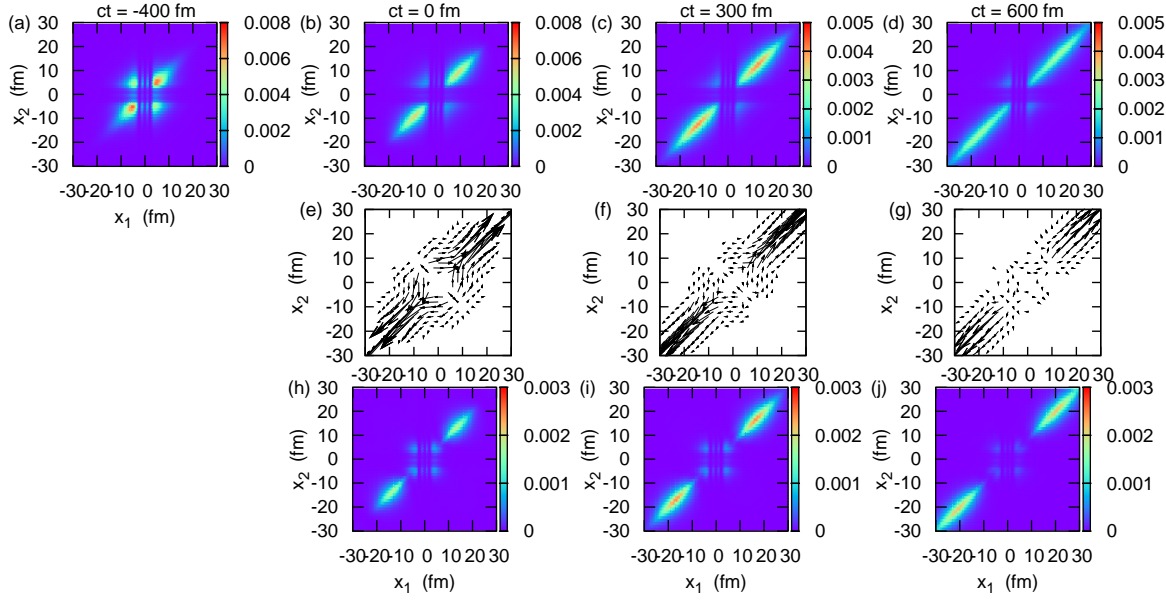


Figure 6. (Color online) The time evolution of the two-particle density. Figs. 6(a), 6(b), 6(c), and 6(d) show the two-particle density, $|\Psi(x_1, x_2)|^2$ at $ct = -400, 0, 300$, and 600 fm, respectively. Figs. 6(e), 6(f), and 6(g) show the corresponding current distributions with arbitrary units. Figs. 6(h), 6(i), and 6(j) show the breakup component of the two-particle density, $|\Psi_{bu}(x_1, x_2)|^2$ at $ct = 0, 300$, and 600 fm, respectively. Notice the difference scales among Figs. 6(a), 6(b), 6(c), and 6(d).

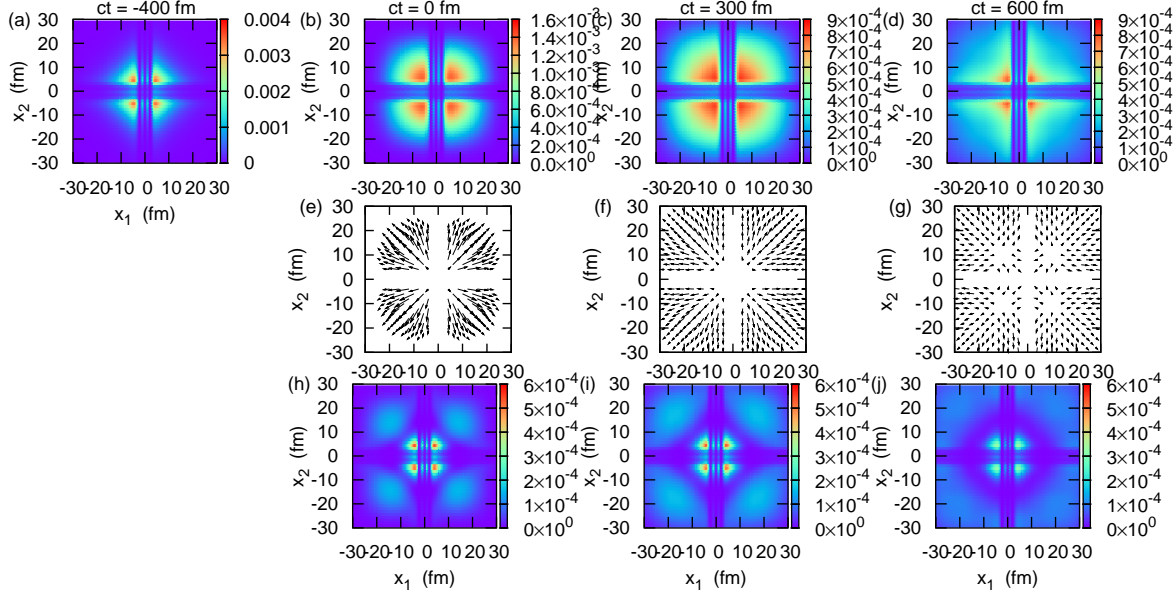


Figure 7. (Color online) Same as Fig. 6, but for the uncorrelated case with a vanishing neutron-neutron interaction. Notice the difference scales among Figs. 7(a), 7(b), 7(c), and 7(d).

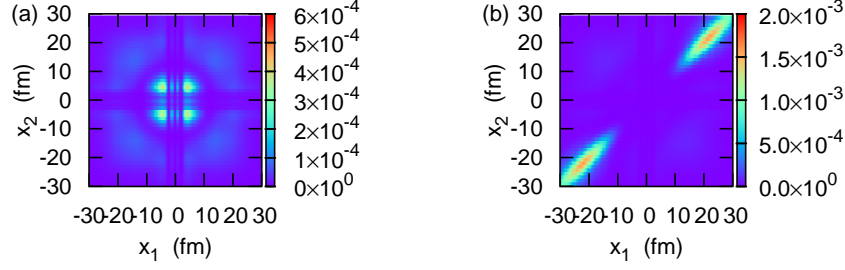


Figure 8. (Color online) The decomposition of the breakup component of two-particle density at $ct = 600$ fm shown in Fig. 6(j). Fig. 8(a) shows the (bc) component, in which one of the neutrons is in a continuum state while the other remains in the bound single-particle state. Fig. 8(b) shows the (cc) component, in which both the two neutrons are in continuum states.

Since there is only one three-body bound state (the ground state) below the dineutron threshold, all the remaining wave functions (20) necessarily correspond to the breakup processes. Figs. 6(h), 6(i), and 6(j) show the time evolution of the breakup component of the two-particle density, $|\Psi_{\text{bu}}(x_1, x_2, t)|^2$. One can clearly see that the two neutrons fly apart from the core nucleus by sticking to each other due to the final state interaction. The effect of the correlation is clearly evidenced by the comparison with the uncorrelated case, shown in Figs. 7(h), 7(i), and 7(j).

In order to clarify the dynamics of breakup process, we further decompose the breakup component of the two-particle wave function into three contributions,

$$\Psi_{\text{bu}}(x_1, x_2, t) = \Psi_{\text{bb}}^{(\text{bu})}(x_1, x_2, t) + \Psi_{\text{bc}}^{(\text{bu})}(x_1, x_2, t) + \Psi_{\text{cc}}^{(\text{bu})}(x_1, x_2, t), \quad (21)$$

where Ψ_{bb} and Ψ_{cc} correspond to the component in which both the neutrons are in the bound single-particle state and in the continuum states, respectively. Ψ_{bc} describes the component in which one of the neutrons is in the bound state while the other is in a continuum state. That is,

$$\Psi_{\text{bb}}^{(\text{bu})}(x_1, x_2, t) = \alpha^{(\text{bu})}(t) \Psi_{00}(x_1, x_2), \quad (22)$$

$$\Psi_{\text{bc}}^{(\text{bu})}(x_1, x_2, t) = \sum_{n \neq 0} \beta_n^{(\text{bu})}(t) \Psi_{0n}(x_1, x_2), \quad (23)$$

$$\Psi_{\text{cc}}^{(\text{bu})}(x_1, x_2, t) = \sum_{\substack{n \leq n' \\ (n, n' \neq 0)}} \gamma_{nn'}^{(\text{bu})}(t) \Psi_{nn'}(x_1, x_2), \quad (24)$$

where $\Psi_{nn'}$ is given by Eq. (6), $n = 0$ corresponding to the bound single-particle level at -0.15 MeV. Figs. 8(a) and 8(b) show the (bc) and (cc) components of the breakup density, $|\Psi_{\text{bc}}(x_1, x_2)|^2$ and $|\Psi_{\text{cc}}(x_1, x_2)|^2$, respectively, at $ct = 600$ fm shown in Fig. 6(j). The (bb) component is small, and is not shown in the figure (the norm of Ψ_{bb} , Ψ_{bc} , and Ψ_{cc} are 4.58×10^{-4} , 0.116 , and 0.466 , respectively. See also Fig. 11 below). It is interesting to notice that the inner part of the density for the (bc) component somewhat resembles the non-correlated density at early times shown in Fig. 7(h). As we will show

in Fig. 10, this originates from the fact that the (bc) component makes a dominant contribution in the uncorrelated case. For the (cc) component, on the other hand, the two emitted neutrons are sticking to each other due to the final state interaction, and the breakup process may be interpreted as an emission of a bound dineutron.

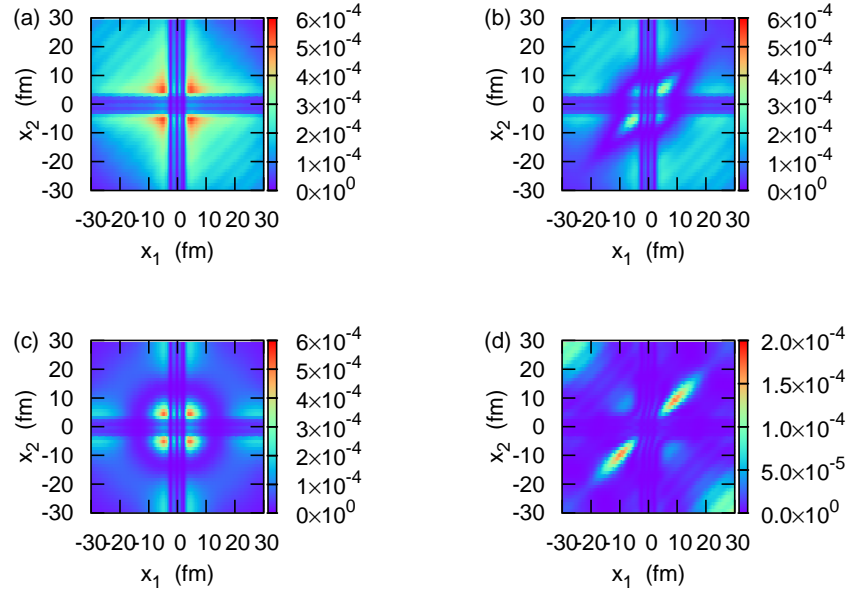


Figure 9. (Color online) The two-particle densities at $ct = 600$ fm obtained by neglecting the final state interaction (*i.e.*, the neutron-neutron interaction) during the time evolution from the correlated ground state at initial time. Figs. 9(a) and 9(b) show the total density, $|\Psi(x_1, x_2)|^2$, and its breakup component, $|\Psi_{bu}(x_1, x_2)|^2$, respectively, while Figs. 9(c) and 9(d) show the (bc) and the (cc) components of the breakup density, respectively.

We point out that both the dineutron correlation in the ground state, as well as the neutron-neutron interaction acting during the time evolution (that is, the final state interaction) are important for the dineutron emission process. In order to demonstrate this, Fig. 9 shows the two-particle density at $ct = 600$ fm obtained by switching off the neutron-neutron interaction during the time evolution. The initial state is still prepared as the correlated ground state. Figs. 9(a) and 9(b) show the total density, $|\Psi(x_1, x_2)|^2$, and its breakup component, $|\Psi_{bu}(x_1, x_2)|^2$, respectively. The (bc) and the (cc) components of the breakup density are also shown in Figs. 9(c) and 9(d), respectively. One can see that the density distributions are considerably different from those corresponding to the fully correlated case, Figs. 6(d), 6(j), 8(a), and 8(b). Without the final state interaction, the probability for the non-correlated two-neutron emission is increased significantly (see the peaks in Figs. 9(a), 9(b) and 9(d) along the $x_1 = -x_2$ line). At the same time, the dineutron emission is somewhat slowed down, as the peaks in Figs. 9(d) along the $x_1 = x_2$ line are located much closer to the core nucleus as compared to the fully correlated case shown in Fig. 8(b).

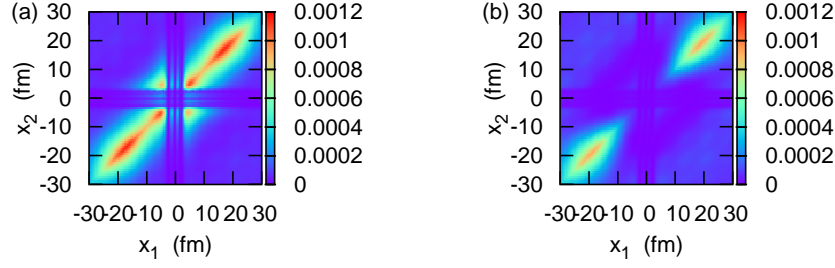


Figure 10. (Color online) Same as Figs. 9(a) and 9(b), but for the case with the final state interaction during the time evolution from the *uncorrelated* ground state at initial time.

Figure 10(a) and 10(b) show the calculated results starting with the *uncorrelated* initial state, but with taking into account the neutron-neutron interaction during the time evolution. To this end, we multiply the same time profile function, $e^{-t^2/2\sigma_t^2}$, as in the time-dependent external field, Eq. 16, to the pairing interaction in the time-dependent Schrödinger equation. Figs. 10(a) and 10(b) show the total density, $|\Psi(x_1, x_2)|^2$, and its breakup component, $|\Psi_{bu}(x_1, x_2)|^2$, respectively. The density along the diagonal $x_1 = x_2$ line now increases significantly, as in the full correlated calculations shown in Figs. 6(d) and 6(j). Evidently, the final state interaction is essential in the breakup processes.

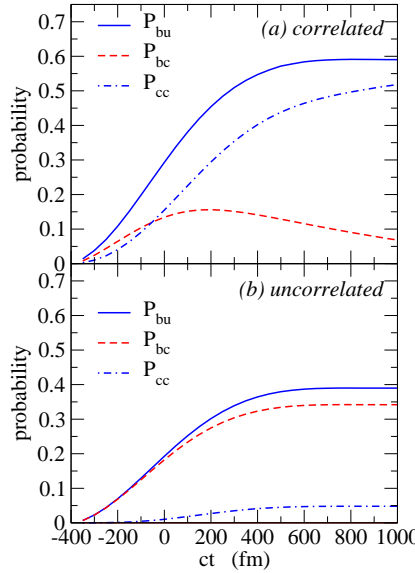


Figure 11. (Color online) The breakup probability as a function of time. The upper and the lower panels correspond to the correlated and the uncorrelated cases, respectively. The solid line shows the total breakup probability, while the dashed and the dot-dashed lines correspond to decompositions of the breakup probability into the (bc) and (cc) processes, respectively. See the text for details.

The total breakup probability as well as the probability for each breakup process are shown in Fig. 10 as a function of time. They are defined as

$$P_{\text{bu}}(t) = \int_{-\infty}^{\infty} dx_1 dx_2 |\Psi_{\text{bu}}(x_1, x_2, t)|^2, \quad (25)$$

$$= |\alpha^{(\text{bu})}(t)|^2 + \sum_{n \neq 0} |\beta_n^{(\text{bu})}(t)|^2 + \sum_{\substack{n \leq n' \\ (n, n' \neq 0)}} |\gamma_{nn'}^{(\text{bu})}(t)|^2, \quad (26)$$

$$P_{\text{bc}}(t) = \int_{-\infty}^{\infty} dx_1 dx_2 |\Psi_{\text{bc}}^{(\text{bu})}(x_1, x_2, t)|^2 = \sum_{n \neq 0} |\beta_n^{(\text{bu})}(t)|^2, \quad (27)$$

and

$$P_{\text{cc}}(t) = \int_{-\infty}^{\infty} dx_1 dx_2 |\Psi_{\text{cc}}^{(\text{bu})}(x_1, x_2, t)|^2 = \sum_{\substack{n \leq n' \\ (n, n' \neq 0)}} |\gamma_{nn'}^{(\text{bu})}(t)|^2, \quad (28)$$

which are denoted by the solid, the dashed, and the dot-dashed lines, respectively. The upper and the lower panels correspond to the correlated and the uncorrelated cases, respectively. Notice $P_{\text{bb}} = 0$ for the uncorrelated case because of the orthogonalization of the wave functions. For the correlated case, although P_{bb} is finite, it is considerably small and is not shown in Fig. 10. By comparing the upper and the lower panels of Fig. 10, one finds that the total breakup probability is increased due to the pairing correlation. This is the case especially for P_{cc} , that is, for the two-neutron emission process.

One also sees that the (bc) component first increases as a function of time while the increase of the (cc) component is somewhat delayed. For the correlated case, the (bc) component eventually decreases and the (cc) component takes over. This is a manifestation of the dominance of a sequential mechanism in the two-neutron breakup, if one intends to use a terminology of perturbation theory. Nevertheless, the strong final state interaction makes the dineutron-like emission the main breakup process as shown in Fig. 6.

In Ref. [17], we have pointed out that the properties of the two-body subsystem with a neutron and the core nucleus play a decisive role in the Coulomb breakup of ^{11}Li and ^6He nuclei. This is because the external field is so weak for the Coulomb breakup that only one of the neutrons makes a transition to other (continuum) single-particle states. This corresponds to the (bc) process in our example. The external field is much stronger for the nuclear breakup process, and the two-step process, or even higher step processes, play an important role. This can be seen in a large probability for the (cc) process, P_{cc} , shown in the upper panel of Fig. 10. The effect of dineutron correlation can therefore be much easily seen in the nuclear breakup process as compared to the Coulomb breakup. A similar conclusion has been reached also in Ref. [51] (see also Ref. [52]).

5. summary

We have developed a simple schematic model for two-neutron halo nuclei, which still contains the essential features of physics of unstable nuclei. The model is based on a

three-body model in one spatial dimension. That is, the two valence neutrons move in a one dimensional mean field potential while interacting with each other via a two-body interaction. The two-body interaction scatters the two neutrons into many single-particle states with opposite parity, causing the strong dineutron correlation in the ground state. Applying this model to a weakly bound two-neutron halo nucleus, we have shown that the two-particle density for the ground state is indeed concentrated in the region of $x_1 \sim x_2$, as a consequence of the dineutron correlation. This model also allows detailed studies on several dynamical processes. We have solved the time-dependent two-particle Schrödinger equation in a non-perturbed way under the influence of a time-dependent external field, which can simulate the field generated by the reaction partner during a heavy-ion collision. We have shown that the main breakup process is an emission of dineutron, that is, the correlated neutron pair, in spite of the one-body nature of the external field and although the one neutron emission process is dominant at the early stage of time evolution. We have also shown that the pairing correlation, and thus the dineutron correlation, significantly enhances the breakup probability, especially for the two-neutron emission process.

A schematic model such as that presented in this paper is useful to get deep insight into the physics behind. In addition to the nuclear breakup process studied in this paper, the one dimensional model for two-neutron halo nuclei can also be used *e.g.*, in order to clarify the pair transfer reactions of exotic nuclei, whose dynamics has not yet been fully understood. A work in this direction is now in progress, and we will publish it in a separate paper [53]. Subbarrier fusion reaction of two-neutron halo nuclei is another interesting application of the one dimensional model. It would be straightforward to extend the one dimensional model for fusion of one-neutron nuclei [54] to two-neutron nuclei. Such study will shed light on the effect of irreversible process such as breakup on many-particle quantum tunneling.

Acknowledgments

K.H. thanks INFN, Sezione di Padova, for its hospitality and financial support. This work was supported by the Grant-in-Aid for Scientific Research (C), Contract No. 22540262 and 20540277 from the Japan Society for the Promotion of Science.

Appendix A. Admixture of even- and odd-parity states

In this appendix, we prove by using a two-level model that α and β in Eq. (14) have the same sign for the density-dependent pairing interaction. These coefficients are determined by diagonalizing a 2×2 matrix,

$$\begin{pmatrix} A & B \\ B & C \end{pmatrix}, \quad (\text{A.1})$$

with

$$A = 2\epsilon_e - \int_{-\infty}^{\infty} dx g(x) \phi_e(x)^4, \quad (\text{A.2})$$

$$B = - \int_{-\infty}^{\infty} dx g(x) \phi_e(x)^2 \phi_o(x)^2, \quad (\text{A.3})$$

$$C = 2\epsilon_o - \int_{-\infty}^{\infty} dx g(x) \phi_o(x)^4, \quad (\text{A.4})$$

$$g(x) \equiv g \left(1 - \frac{1}{1 + e^{(|x|-R)/a}} \right), \quad (\text{A.5})$$

(see Eq. (7)). The lower eigenvalue of this matrix is,

$$\lambda = \frac{1}{2} \left[(A + C) - \sqrt{(A - C)^2 + 4B^2} \right], \quad (\text{A.6})$$

and the corresponding eigenvector is

$$\begin{pmatrix} \alpha \\ \beta \end{pmatrix} = \mathcal{N} \cdot \begin{pmatrix} 2B \\ (C - A) - \sqrt{(C - A)^2 + 4B^2} \end{pmatrix}, \quad (\text{A.7})$$

where \mathcal{N} is the normalization coefficient. Since both B and $(C - A) - \sqrt{(C - A)^2 + 4B^2}$ are negative, α and β have the same sign, as in the BCS ground state wave function in which all the configurations are superposed coherently.

References

- [1] Tanihata I 1995 *Prog. Part. Nucl. Phys.* **35** 505
- [2] Jonson B 2004 *Phys. Rep.* **389** 1
- [3] Hansen P G and Jonson B 1987 *Europhys. Lett.* **4** 409
- [4] Bertsch G F and Esbensen H 1991 *Ann. Phys. (N.Y.)* **209** 327
- [5] Zhukov M V, Danilin B V, Fedorov D V, Bang J M, Thompson I J, and Vaagen J S 1993 *Phys. Rep.* **231** 151
- [6] Jensen A S, Riisager K, Fedorov D V, and Garrido E 2004 *Rev. Mod. Phys.* **76** 215
- [7] Tanihata I *et al.* 1985 *Phys. Rev. Lett.* **55** 2676; 1985 *Phys. Lett.* **160B** 380
- [8] Kobayashi T *et al.* 1988 *Phys. Rev. Lett.* **60** 2599
- [9] Otsuka T, Fujimoto R, Utsuno Y, Brown B A, Honma M, and Mizusaki T 2001 *Phys. Rev. Lett.* **87** 082502
- [10] Fukuda N *et al.* 2004 *Phys. Rev.* **C70** 054606
- [11] Aumann T *et al.* 1999 *Phys. Rev.* **C59** 1252
- [12] Nakamura T *et al.* 2006 *Phys. Rev. Lett.* **96** 252502
- [13] Bertulani C A and Hussein M S 2007 *Phys. Rev.* **C76** 051602(R)
- [14] Hagino K and Sagawa H 2007 *Phys. Rev.* **C76** 047302
- [15] Esbensen H, Bertsch G F and Hencken K 1997 *Phys. Rev.* **C56** 3054
- [16] Hagino K and Sagawa H 2005 *Phys. Rev.* **C72** 044321
- [17] Hagino K, Sagawa H, Nakamura T, and Shimoura S 2009 *Phys. Rev.* **C80** 031301(R)
- [18] Myo T, Kato K, Toki H, and Ikeda K 2007 *Phys. Rev.* **C76** 024305
- [19] Matsumoto T, Hiyama E, Ogata K, Iseri Y, Kamimura M, Chiba S and Yahiro M 2004 *Phys. Rev.* **C70** 061601(R)
- [20] Matsumoto T, Egami T, Ogata K, Iseri Y, Kamimura M and Yahiro M 2006 *Phys. Rev.* **C73** 051602(R)
- [21] Matsumoto T, Kato K and Yahiro M 2010 *Phys. Rev.* **C82** 051602(R)
- [22] Rodriguez-Gallardo M, Arias J M, Gomez-Camacho J, Johnson R C, Moro A M, Thompson I J and Tostevin J A 2008 *Phys. Rev.* **C77** 064609
- [23] Rodriguez-Gallardo M, Arias J M, Gomez-Camacho J, Moro A M, Thompson I J and Tostevin J A 2009 *Phys. Rev.* **C80** 051601(R)

- [24] Ogawa Y, Kido T, Yabana K and Suzuki Y 2001 *Prog. Theo. Phys. Suppl.* **142** 157
- [25] Bertsch G F, Hencken K and Esbensen H 1998 *Phys. Rev.* **C57** 1366
- [26] Baye D, Capel P, Descouvemont P and Suzuki Y 2009 *Phys. Rev.* **C79** 024607
- [27] Hagino K, Sagawa H, Carbonell J, and Schuck P 2007 *Phys. Rev. Lett.* **99** 022506
- [28] Matsuo M, Mizuyama K, and Serizawa Y 2005 *Phys. Rev.* **C71** 064326
- [29] Pillet N, Sandulescu N, and Schuck P, 2007 *Phys. Rev.* **C76** 024310
- [30] Matsuo M 2006 *Phys. Rev.* **C73** 044309
- [31] von Oertzen W and Vitturi A 2001 *Rep. Prog. Phys.* **64** 1247
- [32] Potel G, Bayman B F, Barranco F, Vigezzi E and Broglia R A, arXiv:0906.4298[nucl-th].
- [33] Tanihata I *et al.* 2008 *Phys. Rev. Lett.* **100** 192502
- [34] Chatterjee A *et al.* 2008 *Phys. Rev. Lett.* **101** 032701
- [35] Lemasson A *et al.* 2009 *Phys. Rev. Lett.* **103** 232701
- [36] Dasso C H and Vitturi A 2009 *Phys. Rev.* **C79** 064620
- [37] Pindzola M S, Griffin D C, and Bottcher C 1991 *Phys. Rev. Lett.* **66** 2305
- [38] Grobe R and Eberly J H 1992 *Phys. Rev. Lett.* **68** 2905; 1993 *Phys. Rev.* **A48** 4664
- [39] Lein M, Gross E K U, and Engel V 2000 *Phys. Rev. Lett.* **85** 4707
- [40] Bender M, Heenen P.-H., and Reinhard P.-G. 2003 *Rev. Mod. Phys.* **75** 121
- [41] Merzbacher E 1998 *Quantum Mechanics*, 3rd ed. (John Wiley & Sons, New York, 1998);
Gasirowicz S 2003 *Quantum Physics*, 3rd ed. (John Wiley & Sons, New York, 2003).
- [42] Pérez-Bernal F and Vitturi A 2009 *AIP Conf. Proc.* **1165** 305
- [43] Vitturi A and Pérez-Bernal F 2010 *Nucl. Phys.* **A834** 428c
- [44] Hagino K, Sagawa H, and Schuck P 2009 *Int. J. of Mod. Phys.* **E18** 2045
- [45] Catara F, Insolia A, Maglione E, and Vitturi A 1984 *Phys. Rev.* **C29** 1091
- [46] Ferreira L, Liotta R J, Dasso C H, Broglia R A and Winther A 1984 *Nucl. Phys.* **A426** 276
- [47] Herzog M W, Civitarese O, Ferreira L, Liotta R J, Vertse T and Sibanda L J 1986 *Nucl. Phys.* **A448** 441
- [48] Lotti P, Cazzola F, Bortignon P F, Broglia R A, and Vitturi A 1989 *Phys. Rev. C* **40** 1791
- [49] Tischler M A, Tonina A, and Dussel G G 1998 *Phys. Rev.* **C58** 2591
- [50] Koonin S E, Davies K T R, Maruhn-Rezwani V, Feldmeier H, Krieger S J, and Negele J W 1977 *Phys. Rev.* **C15** 1359
- [51] Assié M and Lacroix D 2009 *Phys. Rev. Lett.* **102** 202501
- [52] Assié M *et al.* 2009 *Eur. Phys. J.* **A42** 441
- [53] Hagino K and Vitturi A, to be published.
- [54] Yabana K and Suzuki Y 1995 *Nucl. Phys.* **A588** 99c